Article

pubs.acs.org/Biomac

Dry-Spun Silk Produces Native-Like Fibroin Solutions

Maxime Boulet-Audet,[†,‡] Chris Holland,[*,†,§] Tom Gheysens,[†,∥] and Fritz Vollrath[†]

[†]Department of Zoology, Oxford University, Oxford, United Kingdom

[‡]Department of Life Sciences, Imperial College London, London, United Kingdom

[§]Department of Materials Science and Engineering, The University of Sheffield, Sheffield, United Kingdom

[∥]Department of Organic and Macromolecular Chemistry, University of Ghent, Ghent, Belgium

Supporting Information

ABSTRACT: Silk's outstanding mechanical properties and energy efficient solidification mechanisms provide inspiration for biomaterial self-assembly as well as offering a diverse platform of materials suitable for many biotechnology applications. Experiments now reveal that the mulberry silkworm *Bombyx mori* secretes its silk in a practically "unspun" state that retains much of the solvent water and exhibits a surprisingly low degree of molecular order (β-sheet crystallinity) compared to the state found in a fully formed and matured fiber. These new observations challenge the general understanding of silk spinning and in particular the role of the spinning duct for structure development. Building on this discovery we report that silk spun in low humidity appears to arrest a molecular annealing process crucial for β-sheet formation. This, in turn, has significant positive implications, enabling the production of a high fidelity reconstituted silk fibroin with properties akin to the gold standard of unspun native silk.

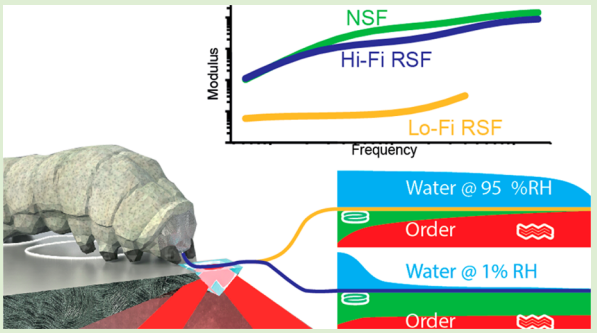

1. INTRODUCTION

The natural silk spinning process entails a silk feedstock experiencing carefully controlled flow stress[1−3] and lowering of pH,[4,5] as well as changing concentrations of metallic ions and salts as it flows down the spinning duct.[5] Thus far, the general perception is that once silk exits the animal, it is "spun" and its natural processing is more or less completed bar some postprocessing draw-down that further aligns the molecules and supramolecular structures.[3,6] However, there is evidence that further molecular self-assembly may continue even after the fiber has left the animal.[2,7,8] To examine the roles of in vivo and ex vivo processing, we examined *Bombyx mori* silk fibers immediately after secretion using infrared spectroscopy. This technique allowed us to monitor the β-sheet and water content of silk fibers in controlled environments in order to infer the molecular processes that might underlie the transition of silk from feedstock to filament.

We propose that through a fundamental understanding of how silk is spun, it is possible to gain technological insights into how to 'unspin' it. Understanding the reverse processing of silk back from solid fiber to liquid feedstock has significant implications for fibroin biomaterial preparation protocols (i.e., reconstitution or regeneration) as they typically overlook the process history of their input silk materials.[9−13] Given that reconstituted silk fibroin (RSF) feedstocks rely on the disruption of the solid silk structure, that is, the highly ordered hydrogen-bonded network of fibroin protein molecules, we hypothesized that silk with lower ordered β-sheet crystalinity content would allow for milder solubilization conditions and produce higher fidelity reconstituted silk feedstocks. We now report that *Bombyx mori* silk is highly hydrated when secreted and that rapid dehydration stops β-sheet formation. This, in turn, makes it possible to produce silk filaments that are more amenable to resolubilization. Indeed, RSF prepared from cocoons spun in a dry environment compared to native silk protein feedstocks taken straight from the gland are spectroscopically and rheologically surprisingly similar, as we shall discuss.

2. METHODS

Experimental Setup for Ex Vivo Monitoring of Silk Fibers. *Bombyx mori* silkworms were reared under laboratory conditions on artificial media until the final instar. Once silkworms started the construction of their cocoon, they were placed inside the environmental chamber of the experimental setup (Figure 1).

We controlled the relative humidity (RH) from 1.0 to 96.0 ± 0.1% and kept the temperature at 25.0 ± 0.1 °C in the environmental chamber via an air tube connected to a Wetsys (Setaram Instrumentation, France) operating at a constant air flow rate of 30 mL/min. The chamber was mounted on top of a Golden Gate Attenuated Total Reflection (ATR) accessory (Specac Ltd., UK) within a Nicolet 6700 Fourier Transform Infrared (FTIR) spectrometer (Thermo Scientific, USA). While spinning its fiber in a figure-of-eight, Figure 1b shows that a silkworm will eventually spin a single silk fiber onto the ATR. Once a fiber was detected via a change

Received: June 16, 2016
Revised: August 5, 2016

DOI: 10.1021/acs.biomac.6b00887
Biomacromolecules XXXX, XXX, XXX−XXX

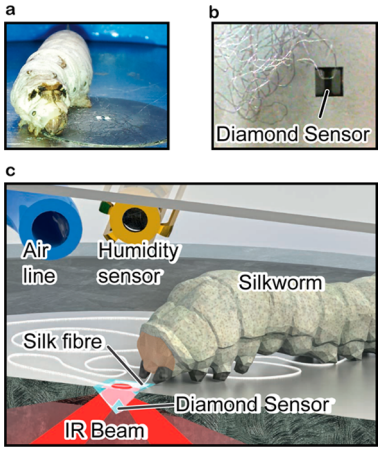

Figure 1. (a) Photograph of a *Bombyx mori* silkworm laying a silk fiber mat to anchor cocoon construction. (b) Single fiber spun directly on the ATR-IR diamond sensor as part of a figure-of-eight pattern. (c) ATR-IR experimental setup showing the *Bombyx mori* silkworm, enclosed chamber with an air inlet and adjacent humidity sensor.

in spectra, we prevented the silkworm from laying additional fibers on the diamond sensor. The internally reflected IR beam probed samples with a penetration depth of ~1 μm over an area of about 1060 × 750 μm (length × width). Infrared spectra collected were mostly representative of the two fibroin filaments (~70% of the mass), but also presented weaker infrared absorption bands at 1395 and 1058 cm^{-1} from the sericin coating (see Figure S1, Supporting Information).[14]

At a 4 cm^{-1} resolution, the spectrometer recorded one spectrum every 0.25 s and averaged four scans for each time frame. Spectra were collected and pretreated using OMNIC 7.3 (Thermo Scientific, Madison, WI). An offset was applied from the average of the 1730–1750 cm^{-1} region and normalized using the side chain region between 1330 and 1450 cm^{-1}. To quantify the dry weight fraction (dry mass/wet mass) from the infrared spectra, 141 silk solutions of varying dry weight fraction between 0% (a control of pure demineralized water) and 95% were measured by infrared spectroscopy. Subsequently, we measured the dry weight fraction of these standard samples by gravimetry after exposure for >12 h under reduced pressure (~100 mbar) in a vacuum oven. Using MATLAB code, we quantified the % dry weight fraction with a partial least-squares (PLS) method using the first derivative of the 1330 to 1550 cm^{-1} region as predictors (i.e., X) against the measured dry weight fraction via gravimetry as responses (i.e., Y), resulting in a model curve with R^2 = 0.973. To quantify the β-sheet crystallinity fraction of the samples, a model was developed from infrared spectra using samples fully converted by methanol exposure, which achieves a maximum crystallinity of 56% based on DSC measurements by Hu et al.[15] We then employed the PLS method to evaluate the first derivative of the 1530 to 1690 cm^{-1} amide I band region, producing a model with R^2 = 0.955. We validated the PLS model using the leave-one-out cross-validation (LOOCV) method where 140 reference spectra were used for the model training, leaving out one spectrum for the validation. The LOOCV is then repeated using a different validation spectrum every time until all 141 spectra are used once.

To monitor solubilization in situ, a droplet of 9.5 M lithium bromide was deposited directly onto dry-spun fibers while collecting FTIR spectra before subsequent washing with demineralized water type II (ρ > 10 MΩ·cm).

Native Feedstock Preparation. To prepare native silk feedstock (NSF), final instar *Bombyx mori* silkworms at the point of spinning had their silk glands extracted and quickly submerged in type II (ρ > 10 MΩ·cm) demineralized water at 22 ± 2 °C, as described in more detail elsewhere.[2] Glands were cut between the sericin-free posterior and posterior-median sections.[16−18] The osmotic pressure expelled a small portion (10 ± 5 μL) of the gland's content from the posterior division within 60 s, enough volume to completely fill the gap of the cone and plate geometry (2.3 μL) of the rheometer. Samples were carefully blotted to remove excess water and were deliberately not trimmed to reduce shear induced artifacts at the edge of the rim.[2] All animal handling in this study conforms to the Animals Act 1986 (Scientific Procedures) of the United Kingdom.

Reconstituted Silk Feedstock Preparation. For convenience, a summary of the following procedures may be found in Table 1. To prepare high fidelity reconstituted silk feedstock (Hi-Fi RSF), final instar *Bombyx mori* silkworms starting to spin were placed in individual cardboard compartments of 2 × 2 × 4 cm separated by steel meshes with 1 mm pore size. The occupied compartments were placed in a sealed plastic box purged with dry air (<4% RH via a AD140L air dryer (PEAK scientific) at room temperature (22 ± 2 °C) and ventilated by a fan. Five days later, cocoons were inverted and cut to remove any spoiled sections of silk and to remove the pupae. Clean, cut cocoons were stored in vacuum-sealed packs at room temperature (22 ± 2 °C) until used. For Hi-Fi RSF, the degumming process differed from standard preparations in that, to remove the sericin, a batch of 10 cocoons were blended for 15 min in 500 mL of demineralized water at room temperature (22 ± 2 °C) using a kitchen food processor. For standard, low-fidelity, reconstituted silk fibroin (Lo-Fi RSF), we used commercially available Chinese *Bombyx mori* cocoons stored at ambient humidity and temperature. We degummed batches of 10 cocoons in 500 mL of a 1% sodium bicarbonate ($NaHCO_3$) solution at 70 °C while blending in a food processor for 30 min.

After degumming, both Hi-Fi and Lo-Fi RSF silk fibers were washed with an excess of demineralized water type II (ρ > 10 MΩ·cm) on top of a 50 μm pore size nylon mesh. Fibers were dried by purging with dry air (<4% RH) at room temperature for 24 h in a custom-built tumble dryer consisting of a rotating plastic tub purged at >5L/min with an AD140L air dryer (PEAK scientific). After drying overnight, the residual water content was estimated to be ~5% by thermogravimetric analysis (TGA).[12] Fibers were again stored in

Table 1. Summary of the Silk Feedstock Preparation Protocols

feedstock preparation step	native silk feedstock (NSF)	high fidelity reconstituted silk feedstock (Hi-Fi RSF)	low fidelity reconstituted silk feedstock (Lo-Fi RSF)
silk sourcing	sericin-free silkworm gland posterior and posterior-median sections	cocoon spun and stored at <4% RH, 22 ± 2 °C <4% RH, 22 ± 2 °C	commercial cocoons stored at ambient humidity and temperature
sericin degumming	↓	blending in demineralized water at 22 °C for 15 min	blending in 1% NaHCOs at 70 °C for 30 min
fiber conditioning	↓	demineralized water washing drying <4% RH, 22 ± 2 °C	
fibroin extraction	↓	0.8 g/mL in 9.5 M LiBr at 70 °C for 10 min dialysis in 10 kDa MWCO at 1 L/h until >2 MQ·cm	
feedstock storage	used within 60 s at 22 ± 2 °C	concentrating to 22% DW at 4 °C sealed in plastic syringe piston at 4 °C	

DOI: 10.1021/acs.biomac.6b00887
Biomacromolecules XXXX, XXX, XXX−XXX

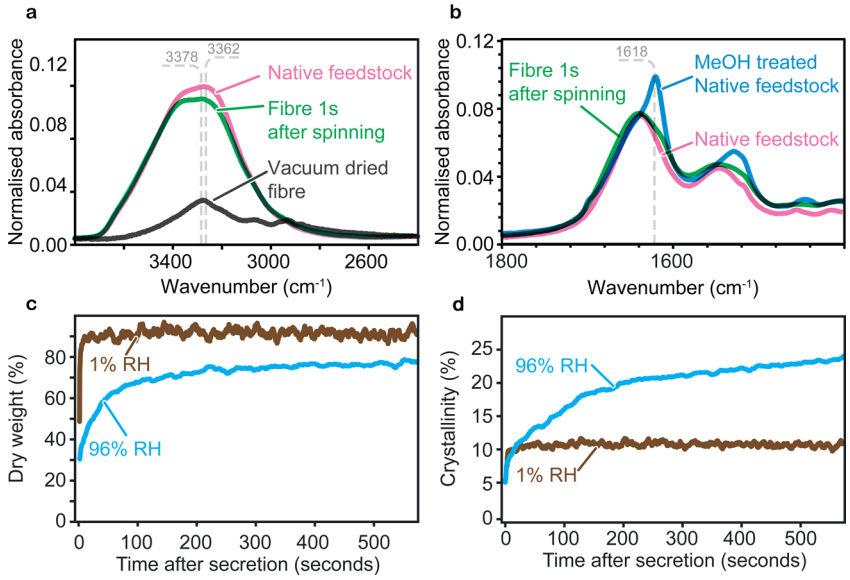

Figure 2. (a) High-wavenumber region infrared spectra of a single fiber immediately after secretion (green) compared to unspun native silk feedstock (pink) and dried fibers (black). (b) Low-wavenumber region infrared spectra of a single fiber immediately after secretion (green) compared to unconverted native silk feedstock (pink) and fully converted feedstock using MeOH (blue). (c) Dry weight fraction and (d) crystallinity fraction of a single fiber immediately after spinning at 1% RH (brown) and 96% RH (blue), as calculated from its infrared spectra.

vacuum packs at room temperature (22 ± 2 °C) until required for dissolution. For both types of RSF, 5 g of degummed silk fibers were dissolved in 20 mL of 9.5 M lithium bromide solution (0.8 g/mL) within a 50 mL centrifuge tube heated to 70 ± 2 °C using a water bath. During fiber dissolution, the mixture was manually stirred gently using a glass rod. After 10 min, the silk/LiBr solution was poured into a dialysis bag of 10 kDa molecular weight cutoff (MWCO) attached at one end to the dispensing portion of a plastic syringe (whose tip was sealed). The dialysis tube-syringe container was then dialyzed in a 1 L vessel against type II (ρ > 10 MΩ·cm) demineralized water at 8 °C using an automatic flushing system at 1 L per hour until the water resistivity reached 2 MΩ·cm. At this point, the dialysis tube-syringe container was hung to dry under a high air flow in a cold room (4 ± 2 °C) until the RSF concentration reached 22 ± 2% dry weight (DW) as measured by gravimetry. Once the desired concentration was reached, the dialysis tube was removed and stored at 4 ± 2 °C, with the dispensing syringe portion containing the RSF sealed with a plastic syringe piston to prevent further evaporation.

Rheo-IR Measurements. Oscillatory, viscosity, and in situ infrared measurements were performed using the Rheo-IR platform described elsewhere.[2] Hi-Fi-RSF (n = 5), Lo-Fi RSF (n = 7), and NSF (n = 4) samples were tested by oscillatory sweeps (623 to 0.623 rad/s, target strain 0.002) and linear shear (0.0018 to 150.6 s^{-1}, $\gamma(t) = 0.0014e^{0.0445t}$). The average of the three highest frequency points of G' gave the plateau modulus G_N, while the five highest viscosity data points informed on the apparent zero shear viscosity η_0. The spectrometer averaged 19 scans per time frame of 5.05 s.

3. RESULTS

To probe the properties of silk fibers as soon as possible after secretion, we exploited the instinctive spinning behavior of the silkworms. Silkworms start cocoon construction by laying a mat of anchoring fibers on surrounding surfaces. We found that a silkworm will readily deposit a fiber on the base that contains the ATR-IR sensor (Figure 1).

Our setup allowed us to spectroscopically measure, for the first time, silk fibers immediately after secretion (Figure 2a,b). The data demonstrated that freshly secreted fibers were nearly as hydrated as the silk feedstock in the gland. The FTIR-based PLS regression method[8] quantified the water content in freshly secreted silk fibers at 69 ± 4% (m/m), close to that of native feedstock at 78 ± 3% (m/m).[2,4] This suggests that silkworm silk dehydrates primarily through evaporation outside the animal, rather than by recovery in the spinning duct, as previously believed.[3]

Further analysis allowed us to calculate fiber β-sheet content after secretion (Figure 2b). We see that not only do freshly secreted fibers have a high water content, but with a weak β-sheet peak at 1618 cm^{-1}, they bear a closer resemblance to unspun native silk feedstock as opposed to silk that has been fully converted by exposure to MeOH. To quantify this similarity, DSC data has previously suggested the maximum fibroin crystallinity fraction to be 56%[15] with noncrystalline sericin constituting ∼30% of secreted fibers.[9,18] This gives a maximum potential fiber crystallinity fraction of our samples to be ∼39%. However, the crystallinity fraction calculated from our FTIR-based PLS indicated that freshly secreted fibers had a crystallinity fraction of only 6 ± 2%, which suggests that the freshly secreted silk contained less than a sixth of the maximum potential β-sheet content. This unexpected finding indicates that the silkworm's spinning apparatus may serve only to trigger, but not complete, silk's conversion/crystallization.

Because fibers appear to dehydrate through evaporation, we predicted that the fiber's water content strongly depends on the ambient relative humidity as well as temperature, air speed and surface area.[19] As shown in Figure 2c, the dry weight fraction of the fiber stabilizes within 600 s in humid air (96% RH). In contrast, flowing dry air (1% RH) evaporated most of the water in the fiber in less than 1 min.

We now propose that, following secretion, the fibers' water content affects the crystallization rate, which is supported by the observation that β-sheet formation can continue spontaneously once triggered,[2,19−21] a phenomenon commonly referred to as water annealing.[22,23] Figure 2d shows that, at 96% RH, β-sheets formed rapidly in the fiber just after secretion before plateauing after several hours to reach a limit of 24 ± 2%. In contrast, fibers spun at 1% RH saw a much slower rate of development of β-sheets, stabilizing at just 10 ± 2% crystallinity

DOI: 10.1021/acs.biomac.6b00887
Biomacromolecules XXXX, XXX, XXX−XXX

fraction. Hence, it is clear that dry-spinning can limit the crystallinity fraction to less than a quarter of the potential β-sheet content.

Given that degree of crystallization relates to water content, we probed this relationship further. Dry silk softens when undergoing a reversible glass transition around 178 °C.[12,20,22,24] However, like nylon[25] and elastin,[26] silk's glass transition temperature (T_g) also depends on the moisture content.[11,12,19,21,27] Adsorbed water molecules lower the T_g by plasticizing the amorphous phase and increase the protein chain mobility, which we predicted may permit reordering of the proteins and allow the crystallization process to proceed (i.e., water annealing).

Thus, to determine the effect of the glass transition on the molecular structure of freshly secreted silk, we rehydrated dry-spun silk fibers by subjecting them to a controlled ramp in humidity (Figure 3a). Figure 3b shows that the dry weight fraction of the fiber decreased with rising air moisture content before plateauing around 83 ± 3% at 96% RH, indicating that the fiber's water content increases with humidity before finally equilibrating.[19]

From a structural perspective, below 76% RH the crystallinity fraction of the fiber remained unaffected (Figure 3c,d). However, upon surpassing 76% RH crystallization resumed quickly as seen by a rise in the characteristic 1608 cm^{-1} β-sheet band.[2] This threshold is consistent with the fiber's reported humidity induced T_g[21,36,37] and X-ray scattering performed on reconstituted silk films.[21] Interestingly, we observed the same humidity related conversion behavior for fibers secreted from the wild silkworm *Saturnia pavonia* (Figure S2 in Supporting Information).

Therefore, as predicted, for dry spun silk fibers, β-sheet formation resumes when exposed above the reported humidity/temperature induced glass transition for silkworm silk.[11,28,29] We conclude that silk fibers continue to crystallize at room temperature above 76% RH within just a few hours. This leads us to propose that practically all commercial sources of *Bombyx mori* silk have already achieved their full β-sheet content during their production, transport and storage. To confirm this inference, we induced silkworms to naturally spin their cocoons in conditions of both high and low humidity.

From the spectra presented in Figure 4, we found that when spun and stored below the T_g, cocoons preserved their low crystallinity (12 ± 2%), whereas wet postspinning storage results in cocoons with 20 ± 2% crystallinity, similar to that of commercial cocoons at 22 ± 2%. This has a profound impact on the preparation of silk-based biomaterials: by inducing silkworms to spin at low RH, we propose that low crystallinity cocoons could be prepared at ambient temperature without the usual chemicals and potentially solubilized under milder conditions.

Degumming involves the removal of a protein, sericin, which coats the silk fiber and serves to bond fibers together in the cocoon. This typically requires boiling cocoons in an alkaline solution for 5 to 90 min.[30−32] It is now widely understood that the heating process reduces the molecular weight of the fibroin.[1,9,10,33,34] The lower average molecular weight distribution results in decreased feedstock viscosity and solid material tensile modulus which could limit their applications.[1,2,10,31,33] By using dry-spun cocoons we found that they can be degummed without heat or additional chemicals via a simple mechanical blending in demineralized water. To confirm the

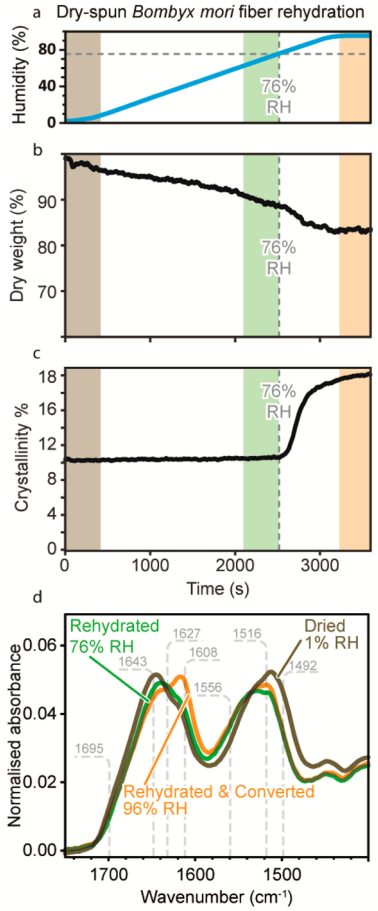

Figure 3. (a) Relative humidity measured by the environment controller during the rehydration of *Bombyx mori* fibers from 1 to 96% at 2% RH/min. (b) Dry weight fraction of a dry-spun *Bombyx mori* fiber under this humidity ramp as calculated from its infrared spectra. (c) Crystallinity fraction of *Bombyx mori* dry-spun fibers under this humidity ramp as calculated from its infrared spectra. (d) FTIR spectra averaged from collection during the shaded time intervals of corresponding color in panels a−c, representing a fiber's dried (light brown), rehydrated (green), and rehydrated/converted (orange) states.

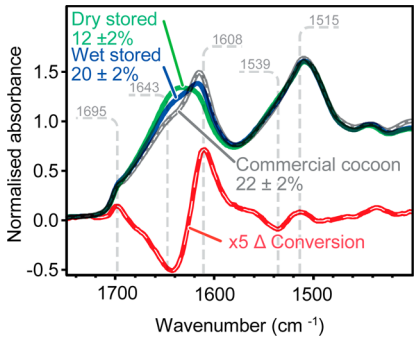

Figure 4. Average infrared spectra of dry stored (green) and wet stored (blue) *Bombyx mori* dry-spun cocoons as well as the difference (red) due to conversion multiplied by a factor of 5 with a spectrum of a commercial cocoon presented as a reference (black) with numbers stated in % representing calculated average crystallinities of silk cocoons (n = 12).

DOI: 10.1021/acs.biomac.6b00887
Biomacromolecules XXXX, XXX, XXX−XXX

removal of sericin once dried, we noted that fibers had lost approximately 30% weight,[18] did not have sericin upon microscopic inspection (data not shown) and did not show any FTIR bands at 1395 and 1068 cm^{-1} that attributed to sericin.[14]

We found that these mechanically degummed low crystallinity fibers could then be solubilized in 70 °C lithium bromide in just 5 min (as opposed to hours as previously reported[32]). Furthermore, it was also possible to solubilize these fibers in LiBr at room temperature (Figure S3 in Supporting Information). Both approaches resulted in a clear "optical grade" RSF.[32]

To assess the quality of this newly created RSF, we compared its rheological properties to standard RSF and unspun native silk fibroin (NSF) at similar concentrations (23 ± 3% DW). Our rheological findings indicate that feedstock prepared from low crystallinity fibers had flow properties remarkably similar to NSF. Thus, we now refer to low crystallinity silk based RSF feedstocks as high fidelity (Hi-Fi) and standard reconstituted silk feedstock as low fidelity (Lo-Fi).

The similarity between Hi-Fi RSF and NSF is highlighted in oscillatory rheology tests, which evaluate the capacity of the feedstock to store and dissipate energy (Figure 5).[1,2] For a

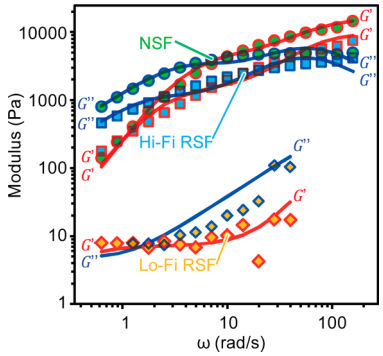

Figure 5. Representative elastic (i.e., storage) modulus G' (red marker outlines) and viscous (i.e., loss) modulus G'' (blue marker outlines) of native silk feedstocks (NSF (green circles)), high-fidelity reconstituted silk feedstock (Hi-Fi RSF (blue squares)) and low-fidelity reconstituted silk feedstocks (Lo-Fi RSF (yellow diamonds)) at comparable 22 ± 3% dry weight fraction. The solid lines represent the best fit of the modulus data using a binary (i.e., two-unit) expressions based on the Maxwellian "springs and dashpots" model.[35,36]

typical polymer melt, the elastic modulus (G') dominates at high frequencies oscillations while the viscous modulus (G'') prevails at lower frequencies. Plotted in Figure 5 and summarized in Table 2, the crossover point where $G' = G''$ occurred for NSF at 10 ± 3 rad/s corresponds to a relaxation time of 0.6 ± 0.1 s. By presenting a crossover at 15 ± 6 rad/s (τ_p = 0.4 ± 0.2 s), our Hi-Fi RSF also displayed a crossover. This is a key finding as, while the crossover is common to NSF, and may in fact be a generic feature,[35,36] it has only once been reported for a recombinant spider silk feedstock, and never for RSF.[37]

Recent rheological work performed on NSF has indicated the presence of relaxation processes, which can be described by parallel Maxwell units.[35,36,38] Applying this approach to our work a two-unit model with two modulus terms (g_3 and g_4) and two relaxation times (τ_3 and τ_4) describes our oscillatory data well and further highlights the similarity between Hi-Fi RSF and NSF (Table 2).[35,36] When Lo-Fi RSF is brought into

Table 2. Summary of the Oscillatory Rheological Results of Silk Feedstock[a]

property	NSF	Hi-Fi RSF	Lo-Fi RSF
g_3 (kPa)	4 ± 2	1.3 ± 0.6	0.06 ± 0.04
τ_3 (S)	0.22 ± 0.05	0.43 ± 0.07	3 ± 1
g_4 (kPa)	11 ± 3	7 ± 2	6 ± 5
τ_4 (s)	0.017 ± 0.001	0.020 ± 0.002	0.010 ± 0.008
τ_p (s)	0.6 ± 0.1	0.4 ± 0.2	
crossover (rad/s)	10 ± 3	15 ± 6	

[a]The error on the calculated moduli values g_3 and g_4 next to the relaxation times τ_3 and τ_4 was obtained from the standard deviation of five measurements.

comparison, it is clear from both Figure 5 and Table 2 that the feedstocks' capacity to store energy is 2 orders of magnitude lower (0.06 ± 0.04 kPa), which largely agrees with previous findings.[1] This is likely a result of the significantly different relaxation mode times brought about by a reduced molecular weight.[1,9,10,33,34]

To determine Hi-Fi RSF's response to shear flow and to mimic flow fields comparable to in vivo spinning,[1,2,34] we subjected samples to an exponential step shear rate ramp while measuring their infrared absorption using our previously developed IR-rheometry platform (Figure 6).[2]

Using rheo-IR,[2] viscosity results confirmed that our Hi-Fi RSF behaved like NSF under shear, implying comparable spinnability.[1] Below 0.1 s^{-1} (region I in Figure 6, upper pane), Hi-Fi RSF had a zero shear viscosity η_0 of 1.0 ± 0.5 kPa·s, much closer to the η_0 of 1.3 ± 0.6 kPa·s for NSF than the 0.09 ± 0.05 kPa·s for Lo-Fi RSF. In this plateau region, the normal force remained constant (middle pane), while no changes in the crystallinity fraction were measured (bottom pane). Region II on Figure 6 shows that Hi-Fi RSF underwent shear thinning and an increase in normal force comparable to that of NSF, while the rheological properties of Lo-Fi RSF did not change significantly. In region II, the center of gravity of the amide II band began to downshift due to the molecular alignment for both NSF and Hi-Fi RSF (Figure S4 in Supporting Information). The lack of infrared absorption change for Lo-Fi RSF suggests that Lo-Fi RSF did not align as much in response to the same shear rate.[1,2]

Upon reaching an instability shear rate ($\dot{\gamma}_i$) of 50 ± 20 s^{-1} (region III), both Hi-Fi RSF and NSF feedstocks rapidly became unstable. Coinciding with an increase in viscosity, the β-sheet crystallinity fraction also started to rise. In contrast, Lo-Fi RSF clearly lacked such transition, suggesting a completely different behavior under the same flow conditions.

For both native silk and Hi-Fi RSF, following the onset of crystallization and subsequent gelation, no further shear can be applied without sample slippage or ejection. We find that when this occurs, native and Hi-Fi RSF only have a crystallinity fraction of 5 to 8%, an amount similar to the β-sheet content we measured in fibers immediately after secretion (Figure 2d). Thus, by subjecting silk feedstocks to the maximum amount of shear stress possible in this mode of deformation, Rheo-IR also corroborates that the majority of β-sheets appear to form by postsecretion water-annealing rather than via shear in the spinning duct.

This is further corroborated by stopping the samples from being sheared further and following their structure development (Figure 6, region IV). We find that post-shearing, silk crystallization continued to increase in both Hi-Fi RSF and

DOI: 10.1021/acs.biomac.6b00887
Biomacromolecules XXXX, XXX, XXX−XXX

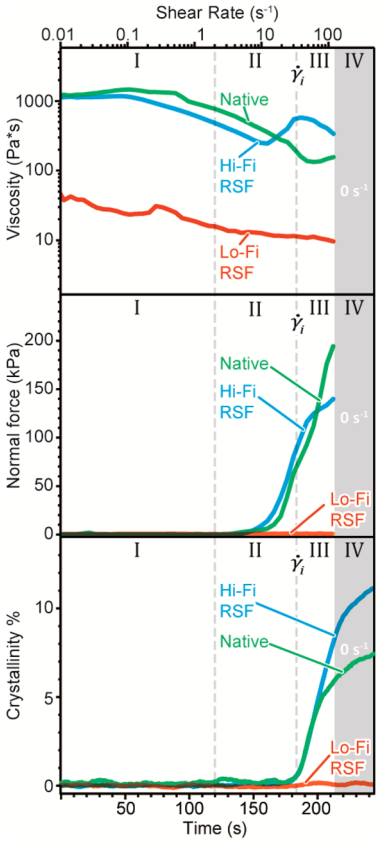

Figure 6. Viscosity, normal force, and crystallinity fraction measured under an exponential shear ramp from 0 to 150 s^{-1} for native silk feedstocks (NSF, (green)), high-fidelity reconstituted silk feedstock (Hi-Fi RSF, (blue)), and low-fidelity reconstituted silk feedstocks (Lo-Fi RSF, (orange)) at 22 ± 3% DW. Shaded area (IV) represents a period of time in which the samples were not sheared but left stationary and structure development monitored. The instability shear rate is denoted by the vertical dotted line and symbol $\dot{\gamma}_i$.

NSF over many hours, akin to our findings for freshly spun silk. These results imply that the solubilization process for Hi-Fi RSF retained silk's natural ability to respond to shear processing and ability to self-assemble, something entirely lacking in the standard Lo-Fi RSF control.

4. CONCLUSIONS

Through our FTIR-based approach we demonstrated that *Bombyx mori* silk fibers immediately after secretion were highly hydrated and dehydrated primarily through evaporation ex vivo. Moreover, immediately after secretion, this silk had less than 15% of the maximum potential β-sheet content in the fiber. By then exposing fibers to different levels of humidity, we found the fibers' crystallinity fraction can be arrested or increased if exposed above the reported humidity/temperature induced glass transition for silkworm silk (~76% RH at ~22 °C). These results imply that water plays a crucial role in the self-assembly of β-sheets and subsequently the level of crystallinity in a fiber.

Moving from single fiber to entire cocoon, we report that by interrupting water annealing through rapid dehydration enables degumming and solubilization under milder conditions during reconstitution. Through the use of rheology, we demonstrated that these improved, high fidelity, reconstituted silk feedstocks exhibited flow properties very similar to native unspun silk and via Rheo-IR, they undergo similar structural transitions in response to flow. This represents a significant technological step forward which we hope will lead to novel fundamental insights into the natural silk production process as well as open the door for new fibroin-based biomaterial applications.[39−44]

■ ASSOCIATED CONTENT

Supporting Information

The Supporting Information is available free of charge on the ACS Publications website at DOI: 10.1021/acs.biomac.6b00887.

Sericin infrared spectra (Figure S1); Dry-spun *Saturnia pavonia* rehydration kinetic (Figure S2); Room temperature dry-spun fiber solubilization in LiBr (Figure S3); Amide band shifts during Rheo-IR shear ramp (Figure S4) (PDF).

■ AUTHOR INFORMATION

Corresponding Author

*E-mail: christopher.holland@sheffield.ac.uk.

Notes

The authors declare no competing financial interest.

■ ACKNOWLEDGMENTS

The authors also wish to thank Rajesh Naik for providing insightful comments on the manuscript and Nick Hawkins for assistance with sample preparation. M.B.-A. is supported by an EPSRC studentship (EP/G068224/1) and a NSERC scholarship (PGS 3D/6799-379132-2009). F.V. acknowledges support from the US-AFOSR (FA9550-12-1-0294) and the European Research Council (SP2-GA-2008-233409). C.H. thanks Magdalen College, Oxford, and the EPSRC (EP/K005693/1) for their support.

■ REFERENCES

(1) Holland, C.; Terry, A. E.; Porter, D.; Vollrath, F. Natural and unnatural Silks. *Polymer* **2007**, *48*, 3388−3392.

(2) Boulet-Audet, M.; Terry, A. E.; Vollrath, F.; Holland, C. Silk protein aggregation kinetics revealed by Rheo-IR. *Acta Biomater.* **2014**, *10* (2), 776−784.

(3) Asakura, T.; Umemura, K.; Nakazawa, Y.; Hirose, H.; Higham, J.; Knight, D. Some Observations on the Structure and Function of the Spinning Apparatus in the Silkworm Bombyx mori. *Biomacromolecules* **2007**, *8* (1), 175−181.

(4) Terry, A. E.; Knight, D. P.; Porter, D.; Vollrath, F. PH induced changes in the rheology of silk fibroin solution from the middle division of Bombyx mori silkworm. *Biomacromolecules* **2004**, *5* (3), 768−772.

(5) Foo, C. W. P.; Bini, E.; Hensman, J.; Knight, D. P.; Lewis, R. V.; Kaplan, D. L. Role of pH and charge on silk protein assembly in insects and spiders. *Appl. Phys. A: Mater. Sci. Process.* **2006**, *82* (2), 223−233.

(6) Dicko, C.; Vollrath, F.; Kenney, J. M. Spider silk protein refolding is controlled by changing pH. *Biomacromolecules* **2004**, *5* (3), 704−710.

(7) Riekel, C.; Madsen, B.; Knight, D.; Vollrath, F. X-ray diffraction on spider silk during controlled extrusion under a synchrotron radiation X-ray beam. *Biomacromolecules* **2000**, *1* (4), 622−626.

(8) Boulet-Audet, M.; Vollrath, F.; Holland, C. Rheo-attenuated total reflectance infrared spectroscopy: a new tool to study biopolymers. *Phys. Chem. Chem. Phys.* **2011**, *13* (9), 3979−3984.

(9) Wray, L. S.; Hu, X.; Gallego, J.; Georgakoudi, I.; Omenetto, F. G.; Schmidt, D.; Kaplan, D. L. Effect of processing on silk-based biomaterials: Reproducibility and biocompatibility. *J. Biomed. Mater. Res., Part B* **2011**, *99B* (1), 89−101.

DOI: 10.1021/acs.biomac.6b00887
Biomacromolecules XXXX, XXX, XXX−XXX

(10) Rnjak-Kovacina, J.; Wray, L. S.; Burke, K. A.; Torregrosa, T.; Golinski, J. M.; Huang, W.; Kaplan, D. L. Lyophilized silk sponges: a versatile biomaterial platform for soft tissue engineering. *ACS Biomater. Sci. Eng.* **2015**, *1* (4), 260−270.
(11) Fu, C. J.; Porter, D.; Shao, Z. Z. Moisture Effects on Antheraea pernyi Silk's Mechanical Property. *Macromolecules* **2009**, *42* (20), 7877−7880.
(12) Guan, J.; Porter, D.; Vollrath, F. Thermally Induced Changes in Dynamic Mechanical Properties of Native Silks. *Biomacromolecules* **2013**, *14* (3), 930−937.
(13) Reed, E. J.; Bianchini, L. L.; Viney, C. Sample selection, preparation methods, and the apparent tensile properties of silkworm (B. mori) cocoon silk. *Biopolymers* **2012**, *97* (6), 397−407.
(14) Boulet-Audet, M.; Vollrath, F.; Holland, C. Identification and classification of silks using infrared spectroscopy. *J. Exp. Biol.* **2015**, *218* (19), 3138−3149.
(15) Hu, X.; Kaplan, D.; Cebe, P. Determining beta-sheet crystallinity in fibrous proteins by thermal analysis and infrared spectroscopy. *Macromolecules* **2006**, *39* (18), 6161−6170.
(16) Machida, J. On the Secretion of the Silk Substances of the Silkworm. *Proceedings of the Imperial Academy* **1926**, *2* (8), 421−422.
(17) Akai, H. The Structure and Ultrastructure of the Silk Gland. *Experientia* **1983**, *39* (5), 443−449.
(18) Gamo, T.; Inokuchi, T.; Laufer, H. Polypeptides of fibroin and sericin secreted from the different sections of the silk gland in Bombyx mori. *Insect Biochem.* **1977**, *7* (3), 285−295.
(19) Agarwal, N.; Hoagland, D. A.; Farris, R. J. Effect of moisture absorption on the thermal properties of Bombyx mori silk fibroin films. *J. Appl. Polym. Sci.* **1997**, *63* (3), 401−410.
(20) Hu, X.; Kaplan, D.; Cebe, P. Effect of water on the thermal properties of silk fibroin. *Thermochim. Acta* **2007**, *461* (1−2), 137−144.
(21) Yazawa, K.; Ishida, K.; Masunaga, H.; Hikima, T.; Numata, K. Influence of Water Content on the beta-Sheet Formation, Thermal Stability, Water Removal, and Mechanical Properties of Silk Materials. *Biomacromolecules* **2016**, *17* (3), 1057−66.
(22) Hu, X.; Shmelev, K.; Sun, L.; Gil, E. S.; Park, S. H.; Cebe, P.; Kaplan, D. L. Regulation of silk material structure by temperature-controlled water vapor annealing. *Biomacromolecules* **2011**, *12* (5), 1686−96.
(23) Jin, H. J.; Park, J.; Karageorgiou, V.; Kim, U. J.; Valluzzi, R.; Kaplan, D. L. Water-stable silk films with reduced beta-sheet content. *Adv. Funct. Mater.* **2005**, *15* (8), 1241−1247.
(24) Yuan, Q.; Yao, J.; Huang, L.; Chen, X.; Shao, Z. Correlation between structural and dynamic mechanical transitions of regenerated silk fibroin. *Polymer* **2010**, *51* (26), 6278−6283.
(25) Miri, V.; Persyn, O.; Lefebvre, J.-M.; Seguela, R. Effect of water absorption on the plastic deformation behavior of nylon 6. *Eur. Polym. J.* **2009**, *45* (3), 757−762.
(26) Samouillan, V.; André, C.; Dandurand, J.; Lacabanne, C. Effect of water on the molecular mobility of elastin. *Biomacromolecules* **2004**, *5* (3), 958−964.
(27) Huang, W.; Krishnaji, S.; Tokareva, O. R.; Kaplan, D.; Cebe, P. Influence of Water on Protein Transitions: Morphology and Secondary Structure. *Macromolecules* **2014**, *47* (22), 8107−8114.
(28) Guan, J.; Vollrath, F.; Porter, D. Two mechanisms for supercontraction in Nephila spider dragline silk. *Biomacromolecules* **2011**, *12* (11), 4030−5.
(29) Wang, Y.; Guan, J.; Hawkins, N.; Porter, D.; Shao, Z. Understanding the variability of properties in Antheraea pernyi silk fibres. *Soft Matter* **2014**, *10* (33), 6321−31.
(30) Yamada, H.; Nakao, H.; Takasu, Y.; Tsubouchi, K. Preparation of undegraded native molecular fibroin solution from silkworm cocoons. *Mater. Sci. Eng., C* **2001**, *14* (1−2), 41−46.
(31) Mo, C. L.; Holland, C.; Porter, D.; Shao, Z. Z.; Vollrath, F. Concentration State Dependence of the Rheological and Structural Properties of Reconstituted Silk. *Biomacromolecules* **2009**, *10* (10), 2724−2728.
(32) Rockwood, D. N.; Preda, R. C.; Yucel, T.; Wang, X. Q.; Lovett, M. L.; Kaplan, D. L. Materials fabrication from Bombyx mori silk fibroin. *Nat. Protoc.* **2011**, *6* (10), 1612−1631.
(33) Partlow, B. P.; Tabatabai, A. P.; Leisk, G. G.; Cebe, P.; Blair, D. L.; Kaplan, D. L. Silk Fibroin Degradation Related to Rheological and Mechanical Properties. *Macromol. Biosci.* **2016**, *16* (5), 666−75.
(34) Wang, Q.; Chen, Q.; Yang, Y.; Shao, Z. Effect of various dissolution systems on the molecular weight of regenerated silk fibroin. *Biomacromolecules* **2013**, *14* (1), 285−9.
(35) Laity, P.; Gilks, S.; Holland, C. Rheological behaviour of native silk feedstocks. *Polymer* **2015**, *67*, 28−39.
(36) Laity, P. R.; Holland, C. Native silk feedstock as a model biopolymer: a rheological perspective. *Biomacromolecules* **2016**, *17*, 2662.
(37) Rammensee, S.; Huemmerich, D.; Hermanson, K. D.; Scheibel, T.; Bausch, A. R. Rheological characterization of hydrogels formed by recombinantly produced spider silk. *Appl. Phys. A: Mater. Sci. Process.* **2006**, *82* (2), 261−264.
(38) Ferry, J. D. *Viscoelastic Properties of Polymers*; Wiley: New York, 1980.
(39) Vepari, C.; Kaplan, D. L. Silk as a biomaterial. *Prog. Polym. Sci.* **2007**, *32* (8−9), 991−1007.
(40) Collins, A. M.; Skaer, N. J. V.; Cheysens, T.; Knight, D.; Bertram, C.; Roach, H. I.; Oreffo, R. O. C.; Von-Aulock, S.; Baris, T.; Skinner, J.; Mann, S. Bone-like Resorbable Silk-based Scaffolds for Load-bearing Osteoregenerative Applications. *Adv. Mater.* **2009**, *21* (1), 75−78.
(41) Omenetto, F. G.; Kaplan, D. L. New opportunities for an ancient material. *Science* **2010**, *329* (5991), 528−31.
(42) Dandu, R.; Ghandehari, H. Delivery of bioactive agents from recombinant polymers. *Prog. Polym. Sci.* **2007**, *32* (8−9), 1008−1030.
(43) Yang, Y.; Ding, F.; Wu, J.; Hu, W.; Liu, W.; Liu, J.; Gu, X. Development and evaluation of silk fibroin-based nerve grafts used for peripheral nerve regeneration. *Biomaterials* **2007**, *28* (36), 5526−35.
(44) Gellynck, K.; Verdonk, P. C. M.; Van Nimmen, E.; Almqvist, K. F.; Gheysens, T.; Schoukens, G.; Van Langenhove, L.; Kiekens, P.; Mertens, J.; Verbruggen, G. Silkworm and spider silk scaffolds for chondrocyte support. *J. Mater. Sci.: Mater. Med.* **2008**, *19* (11), 3399−3409.

DOI: 10.1021/acs.biomac.6b00887
Biomacromolecules XXXX, XXX, XXX−XXX